CHAPTER 6

Pyrene Schiff base derived AIE-active hybrid fluorophore material for potential live cell imaging applications.

6.1 Introduction

Aggregation-induced emission (AIE)-based materials have enthralled consideration due to their wide solicitations in the field of chemistry, biology, and material science [Hong *et al.* (2011), Luo *et al.* (2001), Hong *et al.* (2009), Wang *et al.* (2010), Goswami *et al.* (2016)]. Organic fluorophore molecules with fluorescent properties in solids and concentrated solutions are relatively sporadic since the extended π-conjugated system leads to π–π stacking and devours excited state energy and the molecules become non-emissive, which are pronounced as an aggregation caused quenching (ACQ) phenomenon [Yuan *et al.* (2010), Nie *et al.* (2017), Chen *et al.* (2015), Noh *et al.* (2010)]. Further, this ACQ effect generates a considerable impediment for organic fluorophores towards original solicitations. To overcome this complication, Tang and co-workers exposed an aggregation-induced emission (AIE) phenomenon and asserted that organic fluorophores, which are non-emissive in an organic solvent, turn out to be emissive in a poor solvent in terms of solubility like water [Luo *et al.* (2001), Kamino *et al.* (2010)]. Moreover, upon progressive increase of the fraction of the poor solvent, the organic fluorophore minimizes the contact with the poor solvent due to the hydrophobic effect which leads to aggregation, in turn restricting the rotation of their bond and opening the non-radiative pathway, and the molecules become emissive [Chen *et al.* (2003), Chen *et al.* (2004), Zhao *et al.* (2011), Parrott *et al.* (2014)]. In general, varieties of fluorophores have specific fluorescence properties, and they may be emissive either in a solid or in a solution, but it is challenging to design and synthesize a fluorophore which could be emissive in both the solid and the solution state. Such fluorophore materials have emissive properties in both the solution and the solid states displaying a wide range of applications such as in chemo/biosensors, fluorescent markers,

photodynamic therapy, and cell imaging processes in the solution state [Wang *et al.* (2012), Nakamura *et al.* (2011), Li, M *et al.* (2017), Qin *et al.* (2014)]. Besides, solid-state emitters have attracted attention towards the field of organic light-emitting devices (OLEDs), sensitizers in solar cells, light-emitting field-effect transistors and solid-state dye emitters [Ning *et al.* (2007), Du *et al.* (2012), Kolemen *et al.* (2010), Deng *et al.* (2016), Yao *et al.* (2014)]. The reasonable causes of the solid and solution state emission of fluorophore molecules are molecular packing such as J-aggregation [Ando *et al.* (1985)], intramolecular restricted rotation (RIR), E–Z isomerization, intramolecular charge transfer (ICT) [Peng *et al.* (2013), Grabowski *et al.* (2003)], intramolecular hydrogen bonding and excited-state intramolecular proton transfer (ESIPT). To date, numerous research groups had been actively involved in the synthesis of new varieties of smart fluorophore materials based on a diverse core skeleton to exhibit the AIE effect and the most commonly used AIE active moieties are tetraphenylethylene (TPE), hexaphenyl silole (HPS) and distyrneanthracene (DSA). However, the synthesis of a novel fluorophore material, which is not only useful to exhibit AIE in the solution and the solid state, but also assembles into a specific morphology is still a challenging task. Most of the fluorophores have some limitations towards AIE and solubility; however, a single AIE system with a dual-mode of response such as a tunable color in solution along with a mechanical response in a solid is still rare and demanding.

A novel hybrid fluorophore Pyrene Thiourea (PRT) has been synthesized based on a condensation reaction of two standard fluorescent hydrophobic–hydrophilic molecules, viz. pyrene, and Urea/Thiourea, with an objective to tune the aggregation-induced emission (AIE) along with the morphology. Pyrene being a hydrophobic, planar extended π-conjugated aromatic hydrocarbon with extraordinary light-harvesting properties in the solution state.

Besides, the highly rigid poly aromatic system provides chemical and thermal stability compared with other chromophores. Owing to the distinct photophysical properties of pyrene, the hybrid PRT dramatically exhibits a fluorescence change from colorless to yellow-green via a blue color upon varying the volume fraction of water (poor solvent) in methanol (good solvent). PRT has exhibited not only AIE but also an outstanding quantum yield (FF) of 97% at a 70% water fraction in methanol (70:30, v/v). We attribute the reason behind the tuning of the AIE and quantum yield to the amassing of hydrophobic pyrene at a specific water fraction. The mechanism involved in the AIE has been well supported by detailed UV-vis, fluorescence, SEM, AFM, DFT, PXRD experiments. Besides, PRT serves as a right candidate for the live-cell imaging of HeLa cells.

6.2 experimental section

6.2.1 Method

6.2.1.1 Synthesis of PRU and PRT

To a methanolic suspension of Pyrene (0.46 g, 2 mmol) one mmol of Thiourea/Urea (0.076g, 1 mmol) was added slowly with constant stirring, resulting in a clear light yellow colored solution obtained after a short interval. The reaction mixture was refluxed for 12 h. The ensuing reaction Mixture was cooled, and Sodium Borohydride was added in small proportions to reduce the reaction mixture *insitu*, resulting in a pale white precipitate. The precipitate was collected and neutralized by dilute Hydrochloric acid in order to obtain reduced Pyrene Thiourea (PRT), and Pyrene Urea (PRU) Derivatives then washed with water recrystallized in acetone to obtain yellow colored stable compound.

6.2.2 Preparation of aggregates

The compound PRT was dissolved in methanol to prepare a stock solution with a concentration of 1 x 10^{-4} M. An aliquot of the methanolic stock solution was transferred to a 10 mL Erlenmeyer flask. A requisite amount of water fraction was added dropwise under vigorous stirring to make the ten sets of methanol-water fractions (f_w) of 0–90% (v/v).

6.2.3 Cell imaging methods

6.2.3.1 Cell culture

The cell line maintained in complete DMEM medium (consist 10% fetal bovine serum, supplemented with 20 mM L-glutamine, 100 units/mL penicillin, and 100 µg/mL streptomycin) at 37 °C under a humidified atmosphere of 5% CO_2. Briefly, 0.8×10^3 cells per well were seeded in cell culture plate and incubated for 24h for adherence.

6.2.3.2 Cell viability assay

0.8×10^3 cells per well were seeded in cell culture plate and incubated for 24h for adherence. After 24h the spent culture medium was replaced by fresh medium containing various concentrations of PRU and PRT nanofibers incubated further for 24 h in a 5% CO_2 humidified atmosphere. The medium was then removed, and 100 µL of fresh medium contained 10µL of 5mg/mL MTT solution was added to each well and incubated further for 2h. Finally, the medium containing MTT was removed, and 100µL of DMSO was added to each well to dissolve the formazan crystals followed by incubation for 30 minutes. The intensity of absorbance was assayed using a micro ELISA plate reader at 570nm. The percent cell viability was calculated concerning control according to the following formula:

% Cell viability = [O.D of treated cells/O.D of Control cells] ×100

6.2.3.3 Cell imaging

Cellular uptake of PRU and PRT nanofibers was observed against breast cancer cells (MDA-MB-231) using fluorescence microscopy. The density of 1×10^5 cells was seeded in 6 well plates and kept for 24h at 37°C in a humidified atmosphere of 5% CO_2. After that, seeded cells were incubated with the fresh medium containing PRU and PRT nanofibers at 50μM/mL and incubate further in time-dependent manner for 4h and 24 h at 37°C in humidified 5% CO_2 incubator. Cells were then washed trice by phosphate-buffered saline (PBS) to eliminate the unbound nanofibers. Finally the image of MDA-MB-231 cells was studied under an inverted fluorescent microscope (Evos FL, Life technologies), and the images got were captured in blue, green and red channels with an excitation.

6.2.4 Instrumentation

FT-IR and electronic absorption spectra were obtained on a PerkinElmer Spectrum 100 and a Thermo scientific EVOLUTION 201 spectrophotometer using quartz cuvettes of 1 cm path length in the wavelength range of 200–700 nm, respectively. The emission spectrum recorded on a Varian CaryEclipse fluorescence spectrophotometer. The ^{1}H NMR spectra recorded on a Bruker AVANCE III HD 500 MHz NMR instrument. The electrospray ionization mass (ESI-MS) spectra were recorded on a Waters (Micromass MS Technologies) Q-Tof Premier TOF MS mass spectrometer. SEM images were captured using a Carl Zeiss EVO/18 Research 2045 instrument. Atomic force microscopy (AFM) images were captured using an NTMDT Solver NEXT Russia. Powder XRD data were collected on a Rigaku SmartLab between angle $2\theta = 5–50^0$.

6.3 Results and discussion

We synthesized hybrid fluorophore PRU and PRT by the Schiff base reaction between Pyrene-1-carboxaldehyde and Urea/Thiourea respectively, followed by reduction with sodium borohydride ($NaBH_4$) and neutralization with dilute HCl. (yield, 80%; Scheme 1).

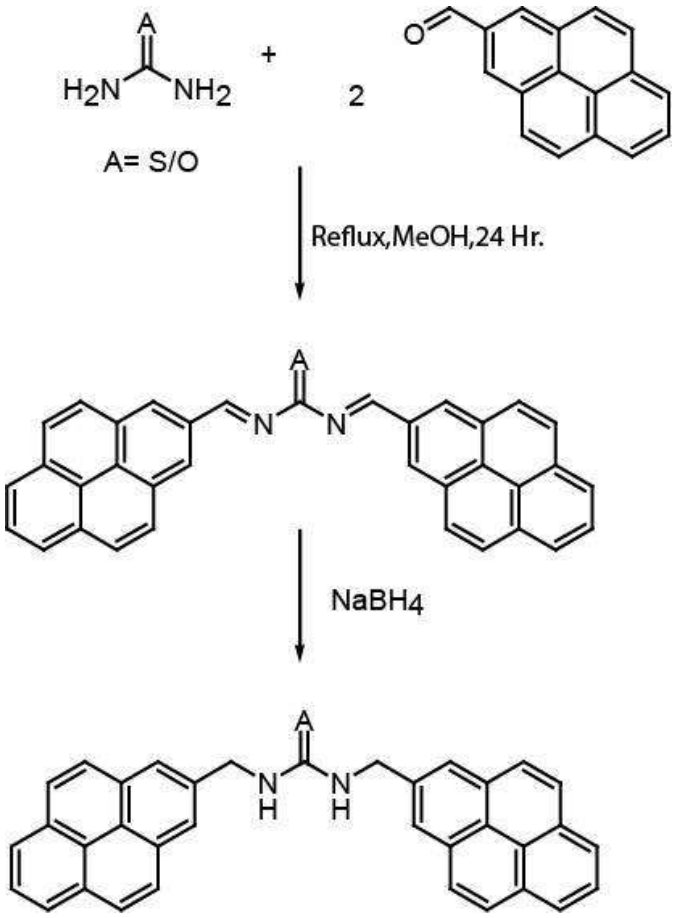

Scheme 6.1 synthetic scheme for prepration of compounds PRT & PRU

6.3.1 Characterization

All the characterization data obtained by various spectroscopic techniques such as FTIR, NMR, ESI-mass, UV-vis absorption, and fluorescence spectrometry are in good agreement with the proposed formulation of the synthesized fluorophores PRU and PRT.

6.3.1.1 ^{1}H NMR of PRT

1H NMR of PRT and PRU were nearly same and carried in deuterated solvent DMSO-d_6 at 500 MHz which showed characteristic peak; 8.39–8.05 (m, 18H pyrene), 5.53–5.25 (s, 1H, NH), 2.50 (m, 4H,CH_2) ppm.

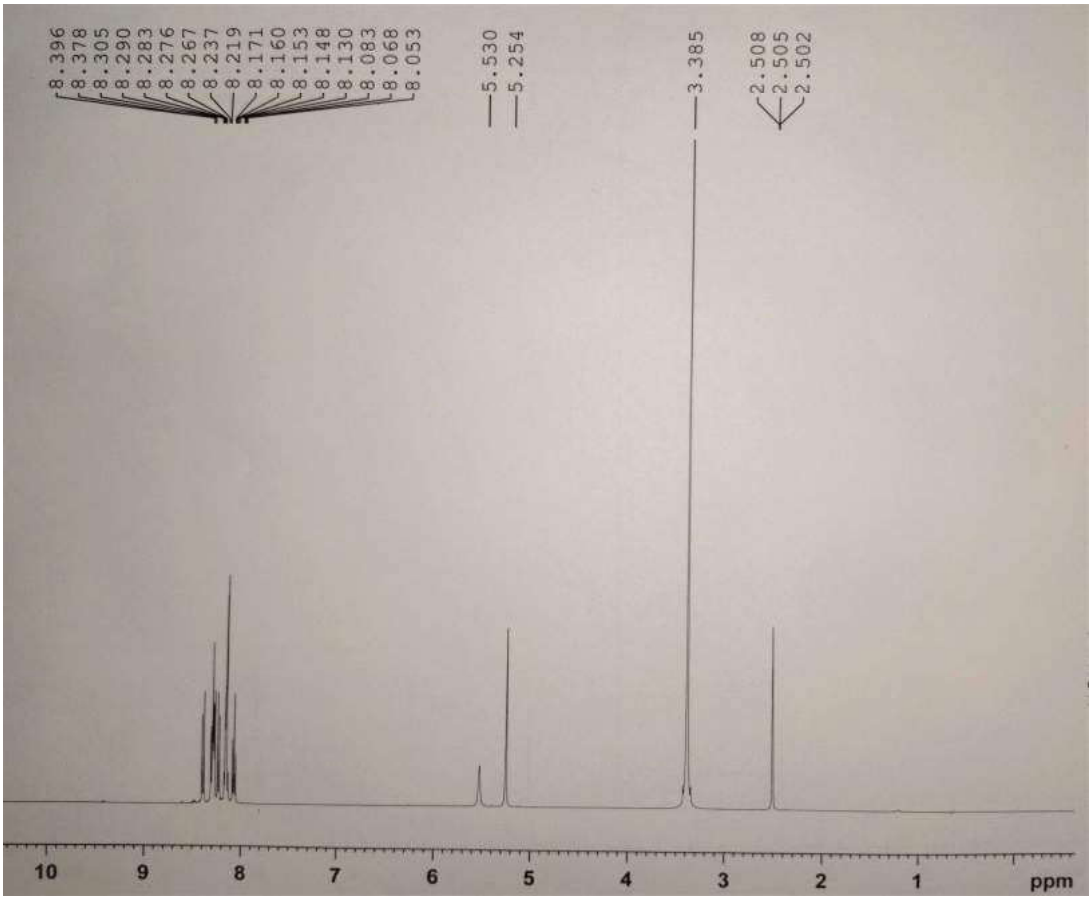

Figure 6.1 ^{1}H NMR analysis of PRT

6.3.2 Optical properties of PRT

6.3.2.1 UV-vis study

The PRT was soluble in methanol, ethanol, DMSO, DMF, THF, chloroform, DCM, and acetonitrile solvents, but was insoluble in water. To monitor the aggregation properties of fluorophore PRT a detailed UV-vis experiment was performed in methanol by varying the percentage of the water fraction (f_w = 0 to 90%). The pure methanolic solution of PRT (c, 1 x10^{-5} M) displayed absorption bands at 274 and 340 nm (figure 6.2). The higher energy band obtained at 278 nm is due to the planar pyrene moiety while the absorption band at 371 nm can be correlated to π–π* transition [Shumate *et al.* (2006)]. Further, upon aliquot increasing the percentage of water in the pure methanolic solution of PRT, the optical density decreases successively without significant change in the position of the bands up to f_w = 90% with a decrease in optical density, which may be due to the extensive aggregation under the influence of the hydrophobic effect. [Huang & Chandler (2002)]

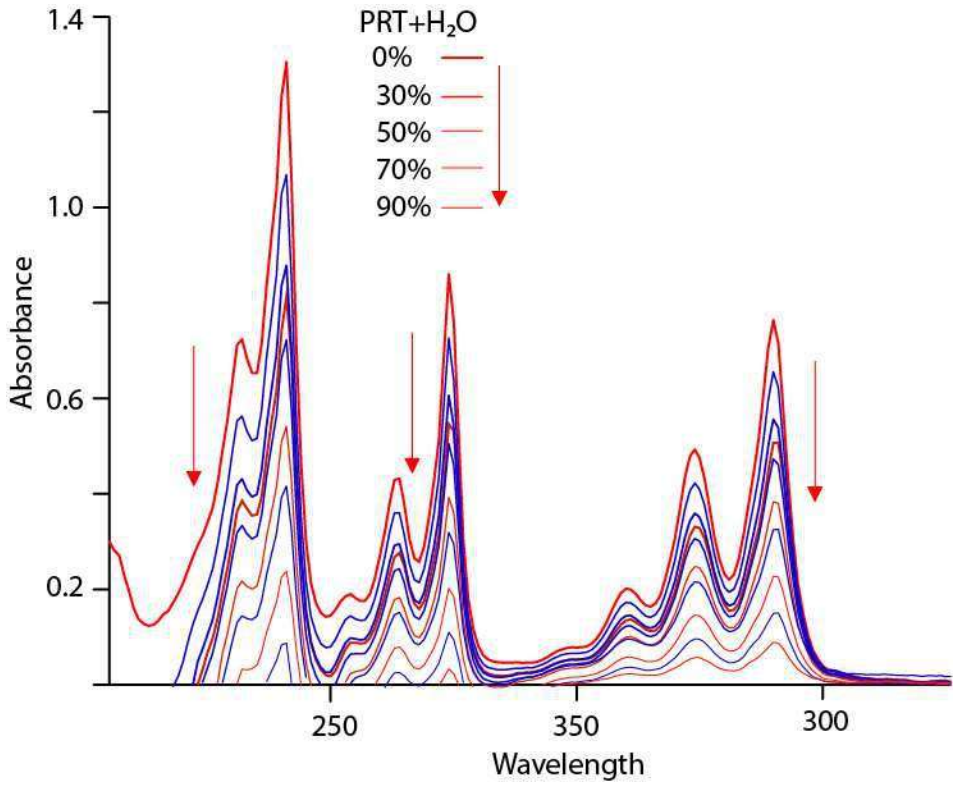

Figure 6.2 UV-visible absorption spectra of PRT at different volume fractions of water

6.3.2.2 Emission study

The emission properties were also investigated to prove the aggregation with an aliquot increment of water fraction in a methanolic solution of PRT (figure 6.3). The methanolic solution of PRT showed an emission band at 468 nm (λ_{ex} = 340 nm, stokes shift = 128 nm) corresponding to the pyrene moiety, and upon gradually increasing the percentage of water up to 80%, the maximum emission intensity attained with a significant hypsochromic shift of 71 nm. The enhancement in intensity with a blue shift may be ascribed to aggregation-induced emission (AIE) and H-type aggregation. With the addition of water up to 80%, the emission corresponding to the excimer decreased dramatically with a hypsochromic shift of 71 nm with the appearance of a much less intense pyrene monomer

emission at 418 nm and a broad band at 446 nm (stokes shift = 78 nm). The origin of the new broad band at 446 nm may be due to the structural change in the pyrene moiety. The references based on pyrene advocate that the addition of 70% water fraction started to quench the fluorescence because the hydrophobic pyrene moieties minimize the contact with water and undergo strong excimer formation (extensive π–π stacking) with an emission band at 468 nm, which can be attributed as ACQ. Remarkably, the spectral change observed was consistent with the visual results obtained under UV light (λ_{ex} = 365 nm) and by the naked eye.

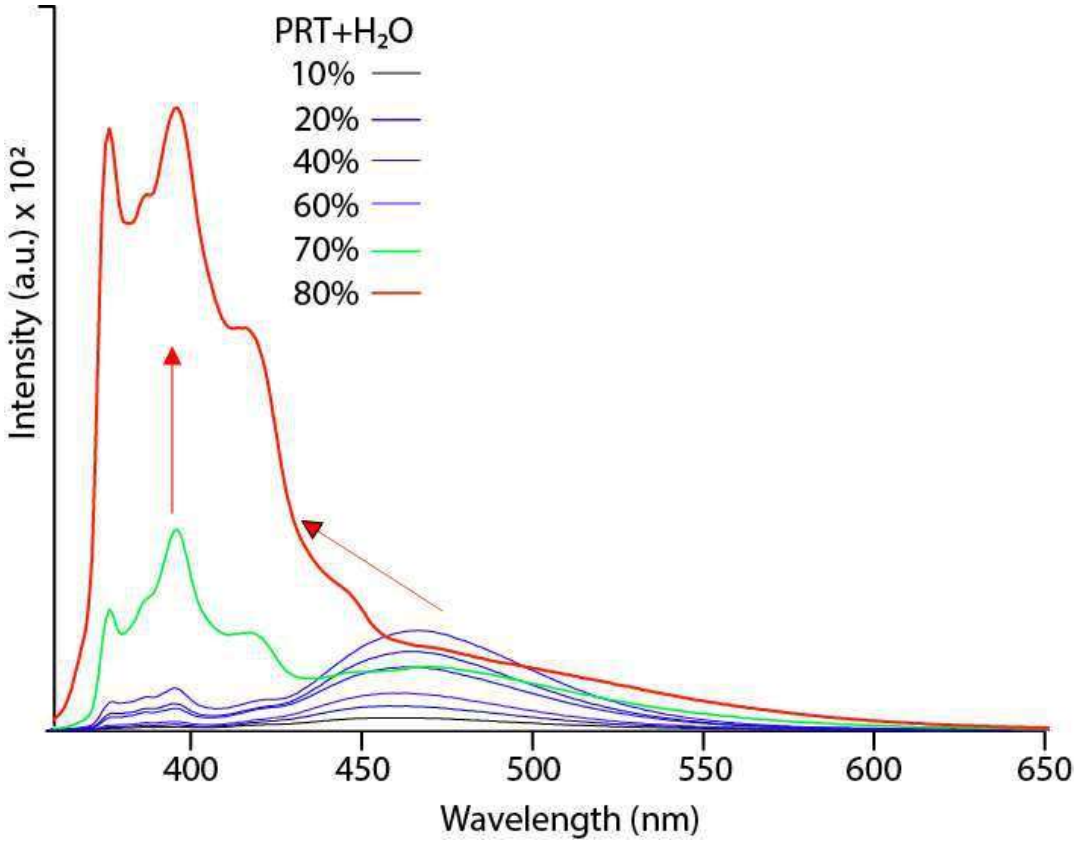

Figure 6.3 Emission spectra of PRT at different volume fractions of water

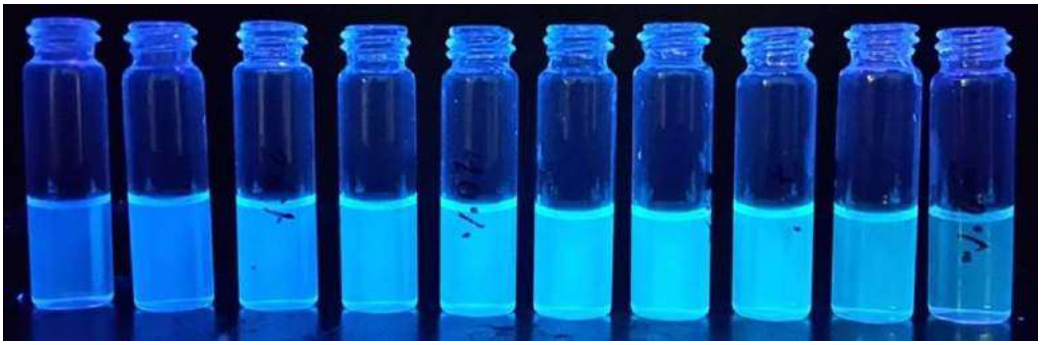

Figure 6.4 Aggregation induced emission was seen at various fractions of water addition with PRT from 10-90% volume increase from left to right in the presence of long-range UV light.

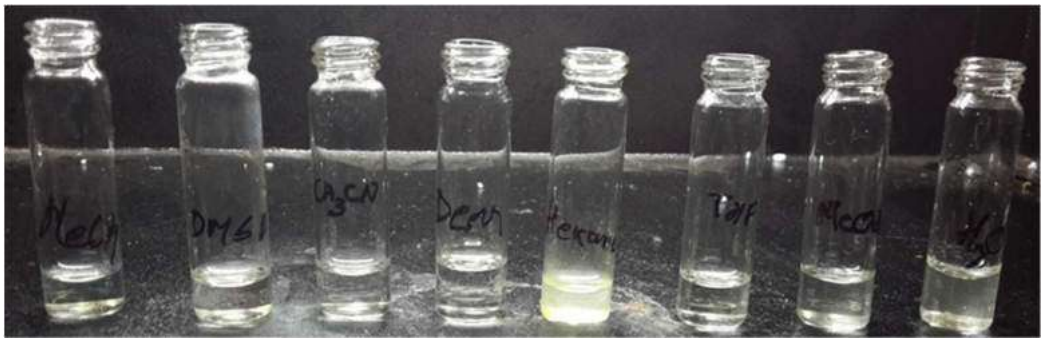

Figure 6.5 PRT in various solvents (Methanol, DMSO, Acetonitrile, DCM, Hexane, THF, Methanol+water, and Water) in visible light only

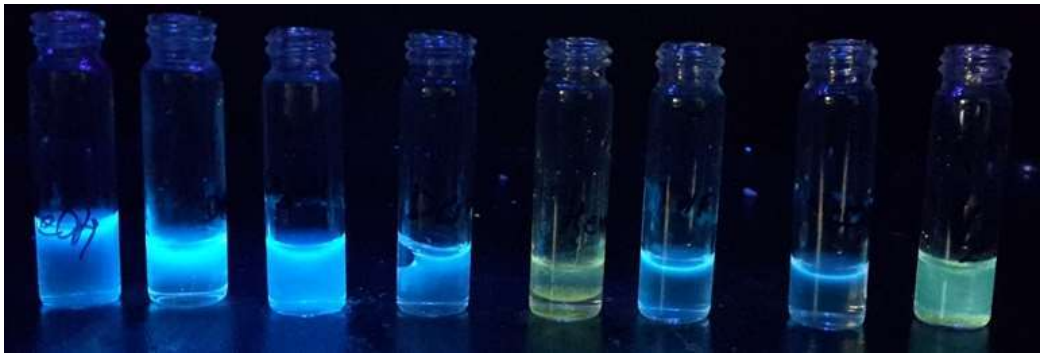

Figure 6.6 Photograph of PRT in various solvents (Methanol, DMSO, Acetonitrile, DCM, Hexane, THF, Methanol+water, and Water) in long-range UV light.

6.3.3 SEM and AFM analysis of aggregate

To monitor the aggregation behavior, morphology, shape, and size of the aggregates. Freshly prepared samples in methanol-water mixtures at water fractions of 10,30,50,70 and 90% are subjected to scanning electron (SEM) (Figure 6.7-6.12) and atomic force microscopy (AFM) analysis (Figure 6.13) . The SEM revealed the formation of nanofibers at 30, 50, and 70% volume fractions of water. Thus, we predicted the arrangement of the hydrophobic (pyrene) units in such a fashion that the pyrene unit is exterior, and the thiourea/urea unit is moved at the interior towards the water to form a fibrous morphology. It is observed that the average size of the nanofibers decreases as the fraction of water increases from 50 to 90%, which may be due to the aforesaid structural changes and extensive aggregation under the influence of critical water fraction [Singh *et al.* (2016)]. The AFM analysis also supports the observation made in SEM about the change in size with increasing the fraction of water from 50% to 90%

6.3.3.1 SEM images

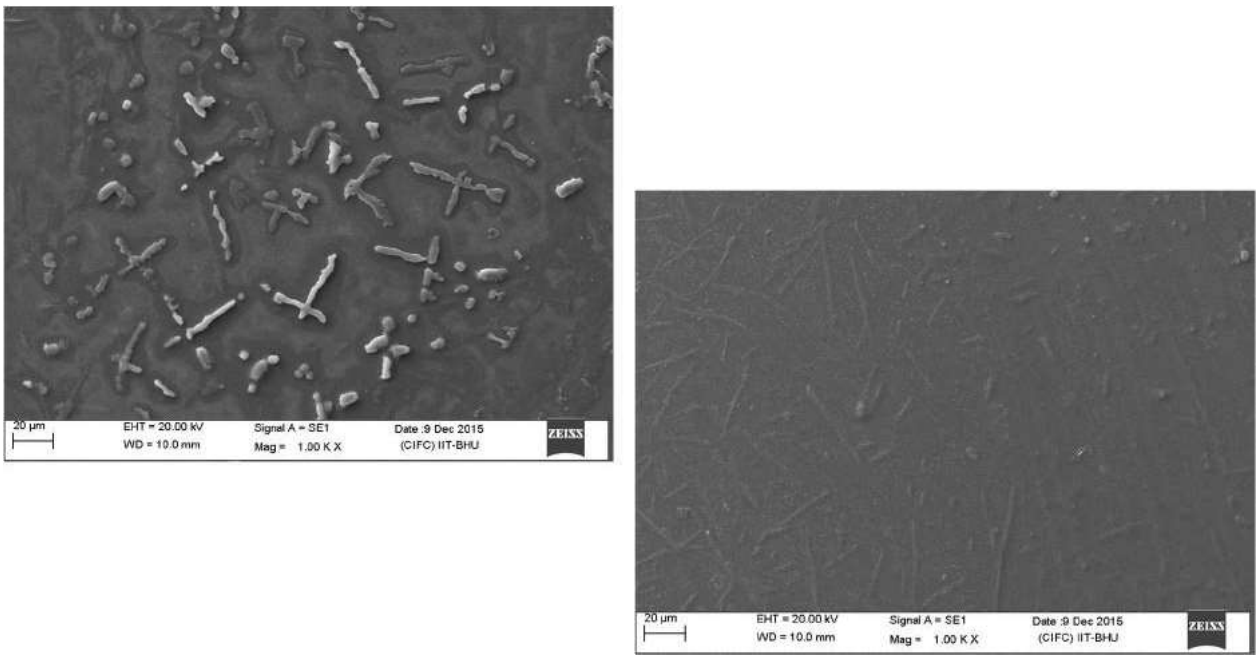

Figure 6.7 SEM images of non-aggregate at 0% volume fraction of water with PRT

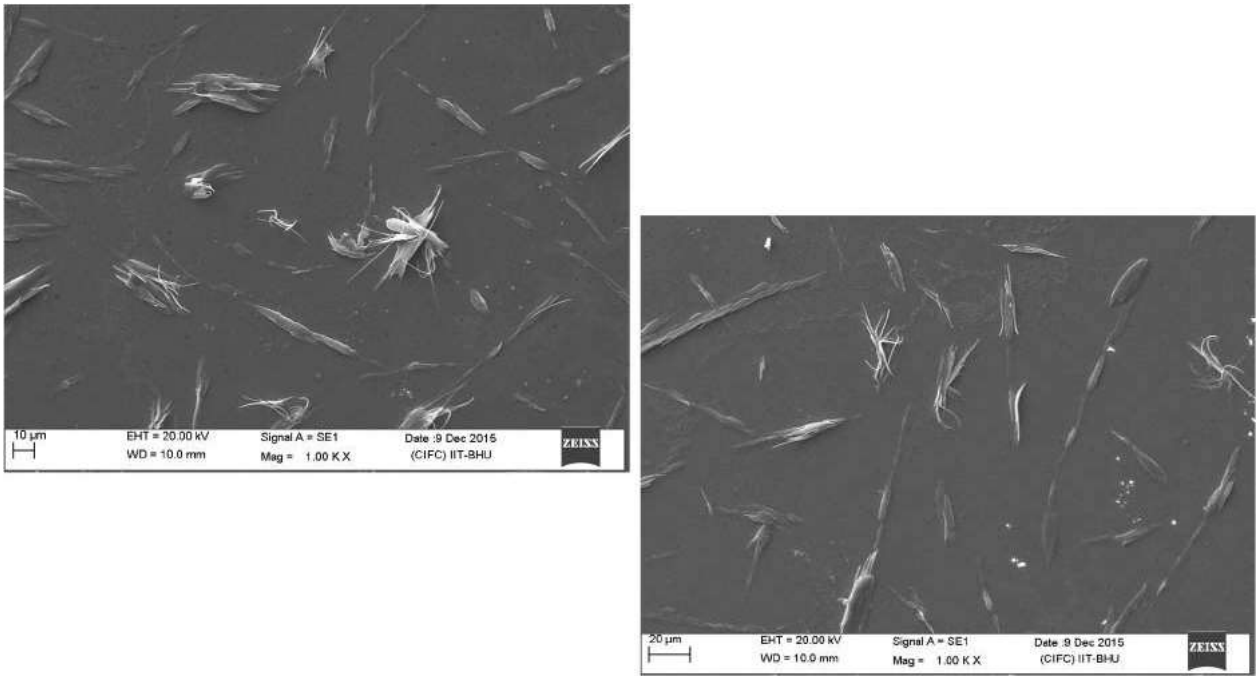

Figure 6.8 SEM images of aggregate formation at 10% volume fraction of water with PRT

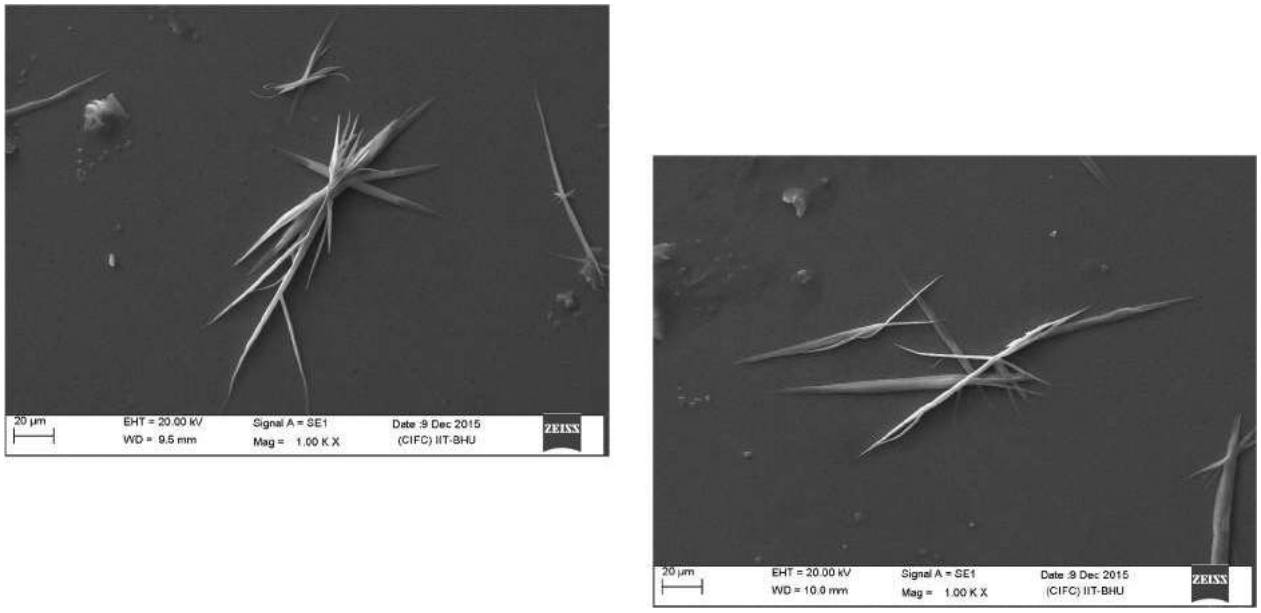

Figure 6.9 SEM images of aggregate formation at 30% volume fraction of water with PRT

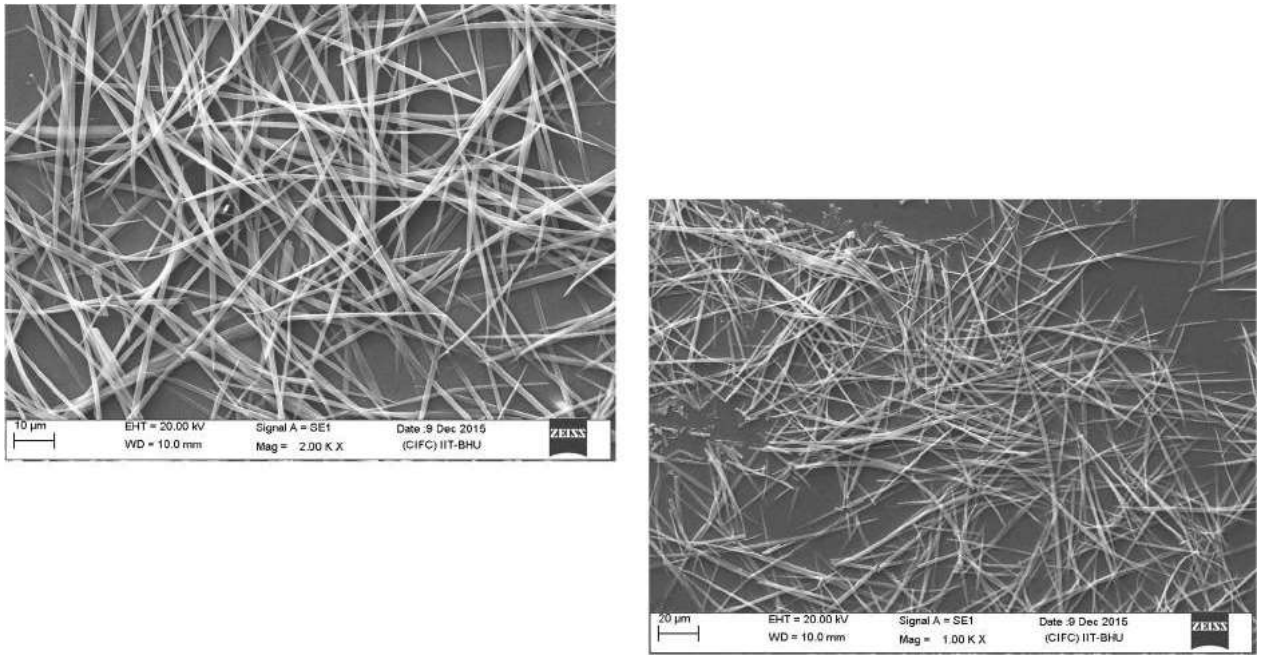

Figure 6.10 SEM images of aggregate formation at 50% volume fraction of water with PRT

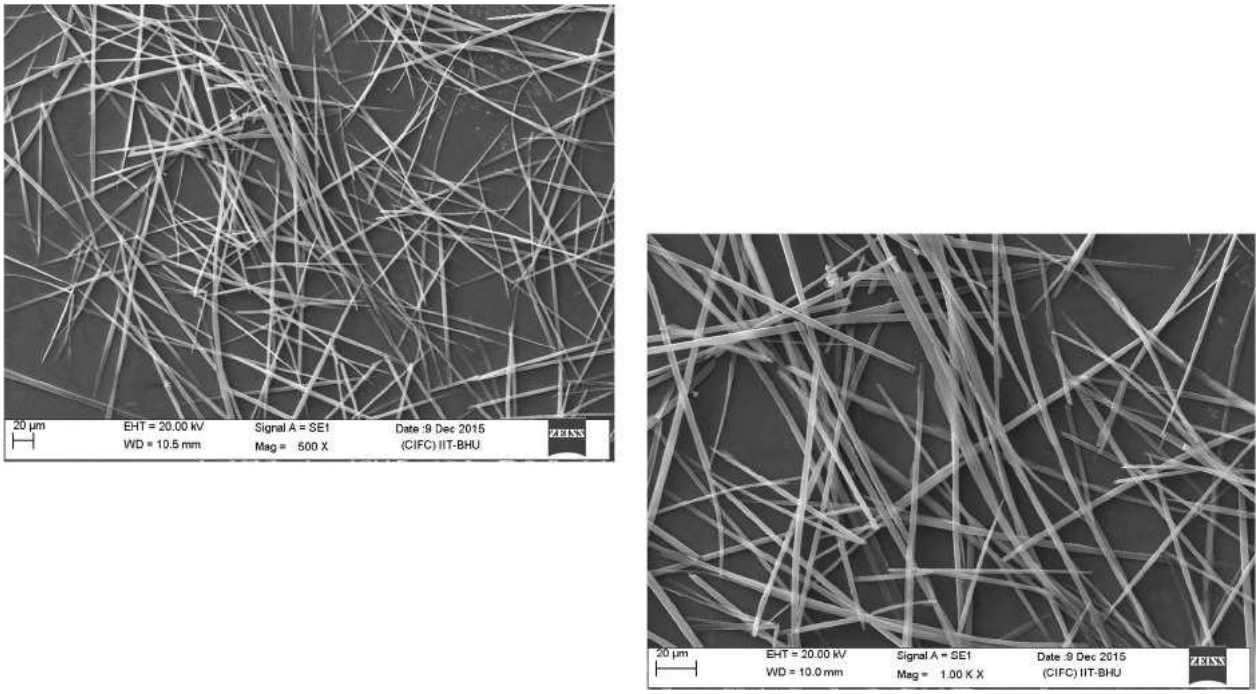

Figure 6.11 SEM images of aggregate formation at 70% volume fraction of water with PRT

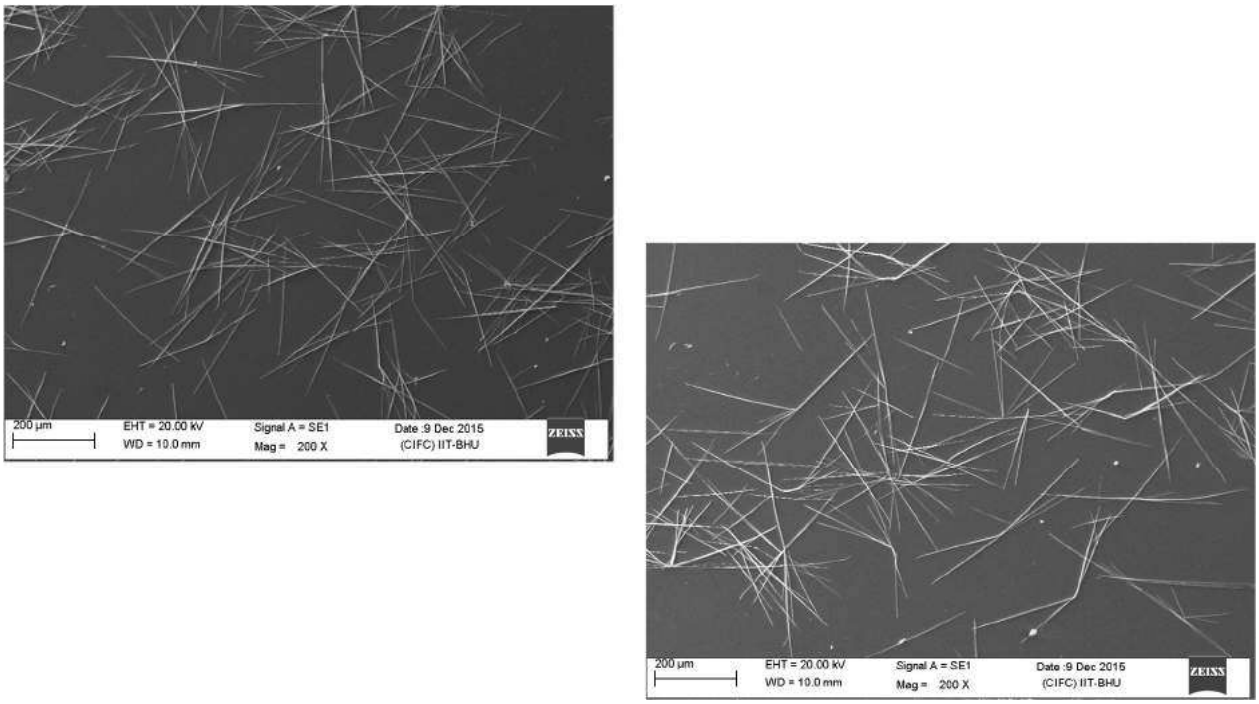

Figure 6.12 SEM images of aggregate formation at 90% volume fraction of water with PRT

6.3.3.2 AFM images

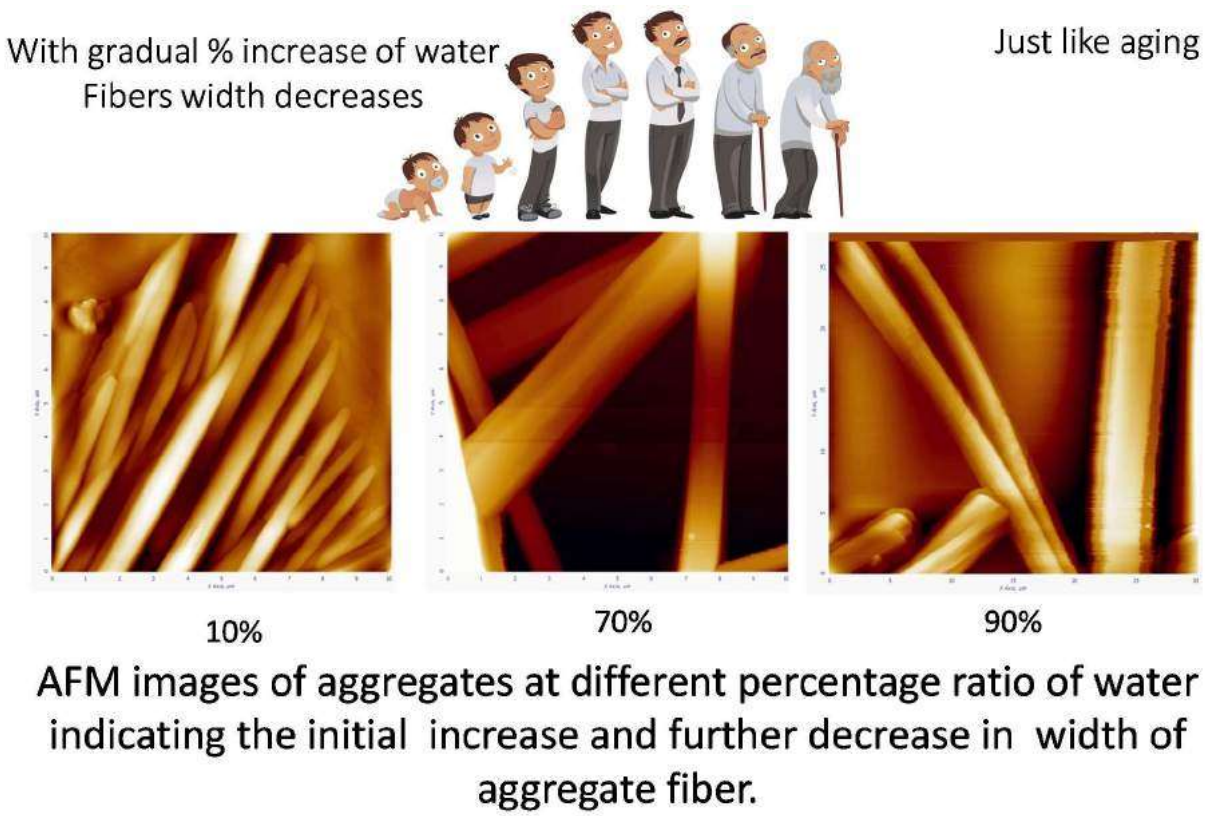

Figure 6.13 AFM images of aggregate formation at a various volume fraction of water with PRT reportedly showing a first increase and then decrease in the aggregation of PRT with Water

6.3.4 PXRD analysis of PRT and aggregate

To gain a better understanding about the mechanism of aggregation and mechanical response, powder X-ray diffraction (PXRD) was acquired before and after the aggregation of PRT samples. The obtained results from PXRD suggest that the crystalline nature of the fluorophore PRT transformed into amorphous upon aggregate formation (figure 6.14). The series of sharp peaks after $2\theta = 30^0$ for non-aggregated PRT suggests the presence of π–π stacking among pyrene moieties. On the other hand, the intensity of the peaks decreased significantly when the aggregated sample was subjected to various fractions of water, which may be due to those mentioned above hydrophilic and hydrophobic region separation during aggregation under the influence of water, resulting in the formation of nanofibrous aggregates with partial crystalline nature.

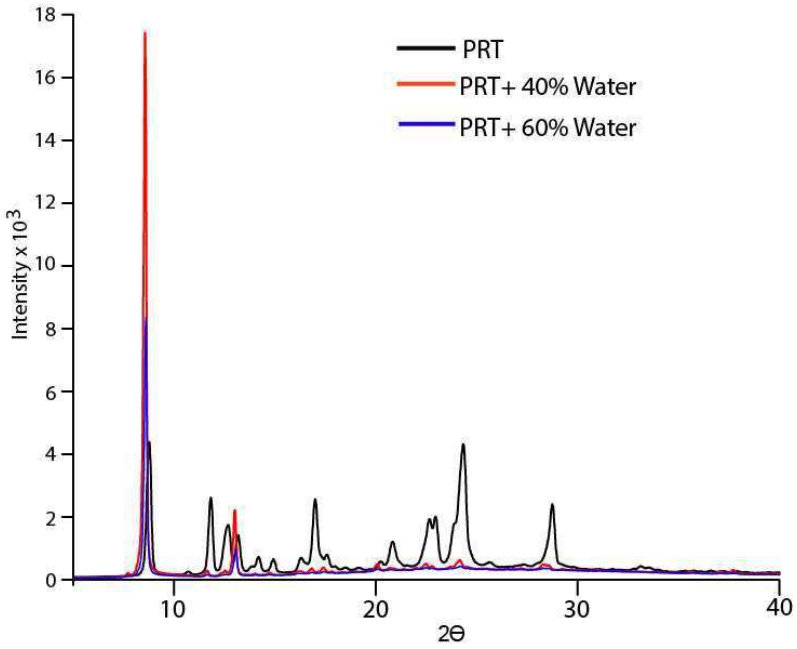

Figure 6.14 PXRD patterns of fluorophore PRT (black line), and its aggregates at 40%(red line) and 60% water fraction (blue line)

6.3.5 NMR Titration

To support the plausible mechanism of aggregate formation, the ^{1}H NMR titration experiment was carried out in DMSO-d_6, and D_2O added as a titrant in 30, 50 and 70% volume fractions (figure 6.15). Notably, DMSO and methanol soluble PRT reveal a similar kind of photophysical behavior under the influence of water. The protons of pyrene appear as a multiplet in the region of 8.35–8.11 ppm, imine at 5.53-5.24 ppm. Up to 30% addition of D_2O, the protons corresponding to pyrene and imine shifted to the upfield region with $\Delta\delta$ = 0.20 and 0.35 ppm, respectively. Thus, it can be concluded from the titration result that the pyrene moiety is involved in the aggregation via π–π stacking, which supports the observation made in fluorescence titration about excimer formation (figure 6.15). The shift in the imine proton maybe because of the involvement in CH–π interaction.

Upon further increasing the fraction to 50% of D_2O, all the peaks either broadened or disappeared, which suggested strong aggregate formation. Thus, we could not analyze the effect of 70% D_2O as observed in fluorescence. Rationally, the ^{1}H NMR titration results are in good agreement with the plausible mechanism proposed based on the fluorescence titration experiment. Thus, based on the available data and results, we depicted the complete arrangement of aggregate formation in figure 6.18.

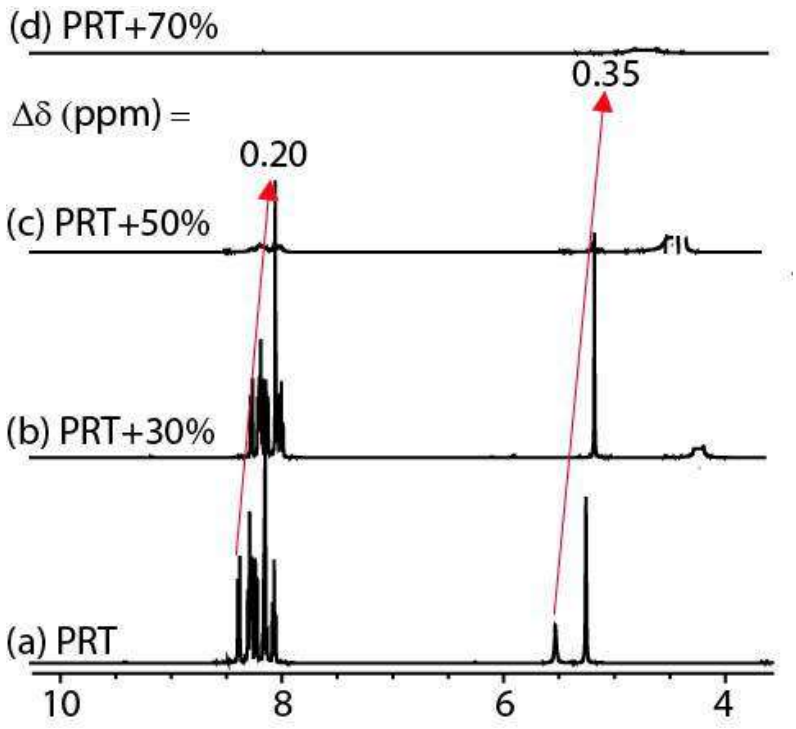

Figure 6.15 ^{1}H NMR titration of PRT with D_2O; aromatic region in ^{1}H NMR spectra (a) PRT free from D_2O, (b) PRT upon addition of 30% D_2O, (c) 50% and (d) 70% D_2O.

6.4 Application of PRT/PRU

6.4.1 Cell viability of PRT

Human breast cancer cell line (MDA-MB-231) is used to check cellular viability and cytotoxicity of PRU and PRT nanofibers using colorimetric assay by MTT (3-(4, 5-dimethylthiazol-2-yl)-2, 5-diphenyl tetrazolium bromide) based on the conversion of yellow tetrazolium salt to purple color formazan crystal by reaction with mitochondrial succinate dehydrogenase of metabolically active cells. The cell line is maintained in complete DMEM

medium (consist 10% fetal bovine serum, supplemented with 20 mM L-glutamine, 100 units/mL penicillin and 100 µg/mL streptomycin) at 37 °C under a humidified atmosphere of 5% CO_2. Briefly, 0.8×10^3 cells per well were seeded in cell culture plate and incubated for 24h for adherence. After 24h the spent culture medium was replaced by fresh medium containing various concentrations of PRU and PRT nanofibers incubated further for 24 h in a 5% CO_2 humidified atmosphere. The medium was then removed and 100 µL of fresh medium contained 10µL of 5mg/mL MTT solution was added to each well and incubated further for 2h. Finally, the medium containing MTT was removed and 100µL of DMSO was added to each well to dissolve the formazan crystals followed by incubation for 30 minutes. The intensity of absorbance was assayed using a micro ELISA plate reader at 570nm [Kathiravan *et al.* (2014)]. The percent cell viability was calculated with respect to control according to the following formula:

% Cell viability = [O.D of treated cells/O.D of Control cells] ×100

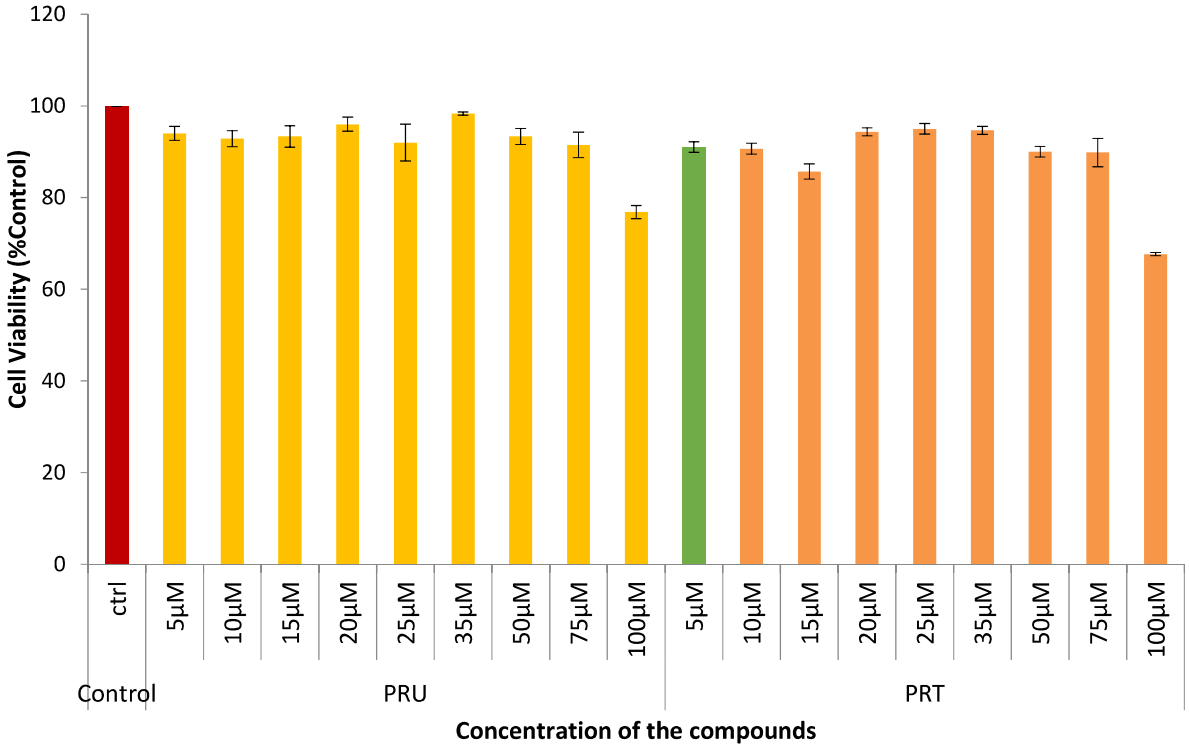

Figure 6.16 MTT assay of both PRU and PRT showing nontoxic behavior of both with various concentrations of PRT and PRU compound for 24 hours. Data were represented as mean SEM from three independent experiments.

6.4.2 Cell Imaging

Cellular uptake of PRU and PRT nanofibers was observed against breast cancer cells (MDA-MB-231) using fluorescence microscopy. The density of 1×10^5 cells was seeded in 6 well plates and kept for 24h at 37°C in a humidified atmosphere of 5% CO_2. After that, seeded cells were incubated with the fresh medium containing PRU and PRT nanofibers at 50µM/mL and incubate further in time-dependent manner for 4h and 24 h at 37°C in humidified 5% CO_2 incubator. Cells were then washed trice by phosphate-buffered saline (PBS) to eliminate the unbound nanofibers. Finally, the image of MDA-MB-231 cells was studied under an inverted fluorescent microscope (Evos FL, Life technologies), and the

images got were captured in blue, green and red channels with an excitation [Xiao *et al.* (2014), Xia & Qian (2016)].

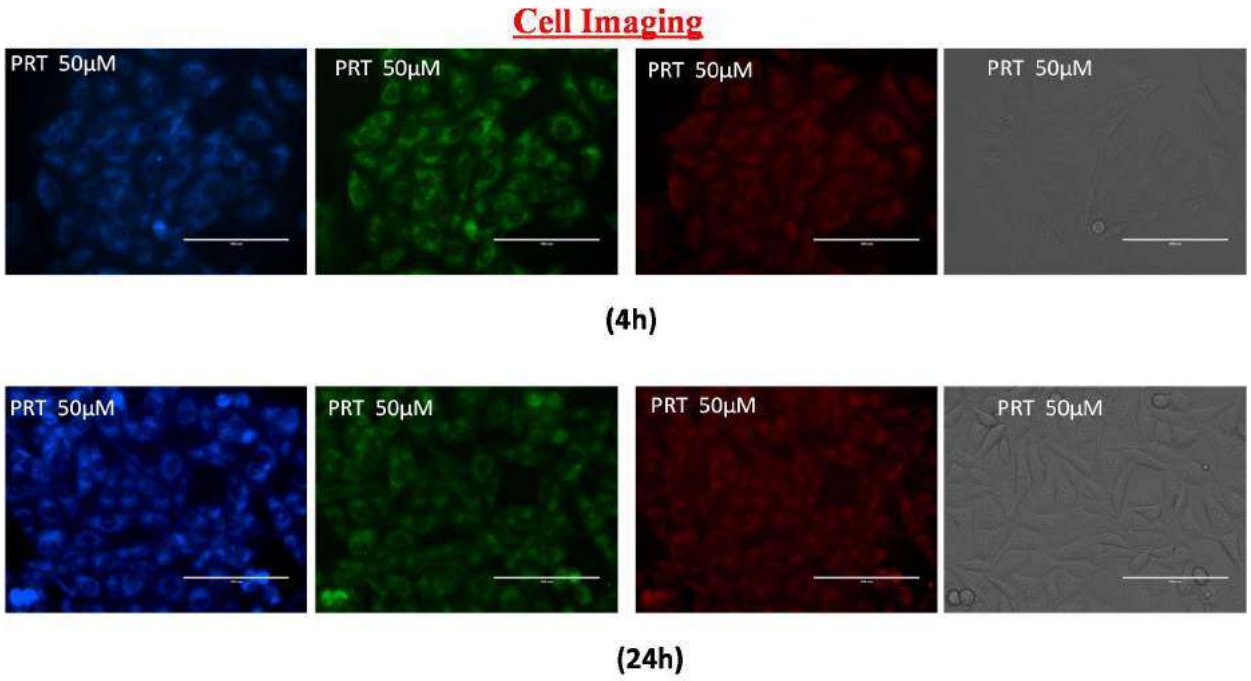

Figure 6.17 the images showing the florescence emitted by MDAMB-231 cells on incubation with PRU and PRT complexes. $1.5x10^5$ Cells treated with the complexes at indicated concentration of (50μM) for 4h and 24h. The images were captured by an inverted fluorescence microscope (EVOS FL, Life technologies).

6.5 Conclusions

In summary, we successfully synthesized the smart fluorophore material PRT and PRU via a simple condensation reaction of 1-pyrenecarboxaldehyde and Thiourea/Urea. Both of them was discovered to be an excellent AIE and color tuner at a critical water fraction of 70%. The results obtained from UV-vis, fluorescence, quantum yield, SEM, AFM, PXRD experiments as well as visual changes under UV light are found to be in good agreement with the proposed mechanism in favor of AIE and color change. The tuning of the color from blue to yellow-green under UV light along with the decrease in the size of the nanofibers were

well established with the extensive aggregation of the pyrene ring. Absorption characteristics of PYRL have been batho-chromatically tuned to the visible region by extending the π-conjugation.

The extended π-conjugation is confirmed and reveals that π→π* transition is the primary factor responsible for electronic absorption.

The photophysical property of PRT was carefully examined in different organic solvents at different concentrations, and intriguingly, the fluorescence intensity of PYRL increases enormously by the gradual addition of water up to 90%.

This signifies that this molecule has aggregation-induced emission (AIE) property. The mechanism of AIE of this molecule is the suppression of photoinduced electron transfer (PET) due to hydrogen bonding interaction of -NH donor with water.

Cell imaging was performed on MDA-MB-231 cell lines by using fluorescent microscopy. Cells were treated with both PRU and PRT nanofibers at 50μM/mL for 4h and 24 h in time-dependent manner. Result represents moderate emission of fluorescence after four hour incubation with both PRU and PRT nanofibers in three fluorescence channels, blue, green, and red in MDA-MB-231 cells. Further, with increasing incubation time for 24 h both nanofibers showed enhanced emission of blue fluorescence in the GFP channel followed by green and red channels due to higher intracellular accumulation of PRU and PRT nanofibers.

In addition to the fluorescence cell imaging, the cell viability and cytotoxic effect of both PRU and PRT nanofibers was performed on MDA-MB-231 cells by using MTT assay. The result of MTT assay showed that PRU and PRT did not induce significant toxicity on

breast cancer cells (MDA-MB-231) even at higher concentration (100µM). The cell viability of MDA-MB-231 cells was found to be maximum (70-80%) at higher concentration (100µM/mL) which indicate that PRU and PRT both nanofibers used as a good candidate in bioimaging with non-toxic and safety properties against breast cancer cells.

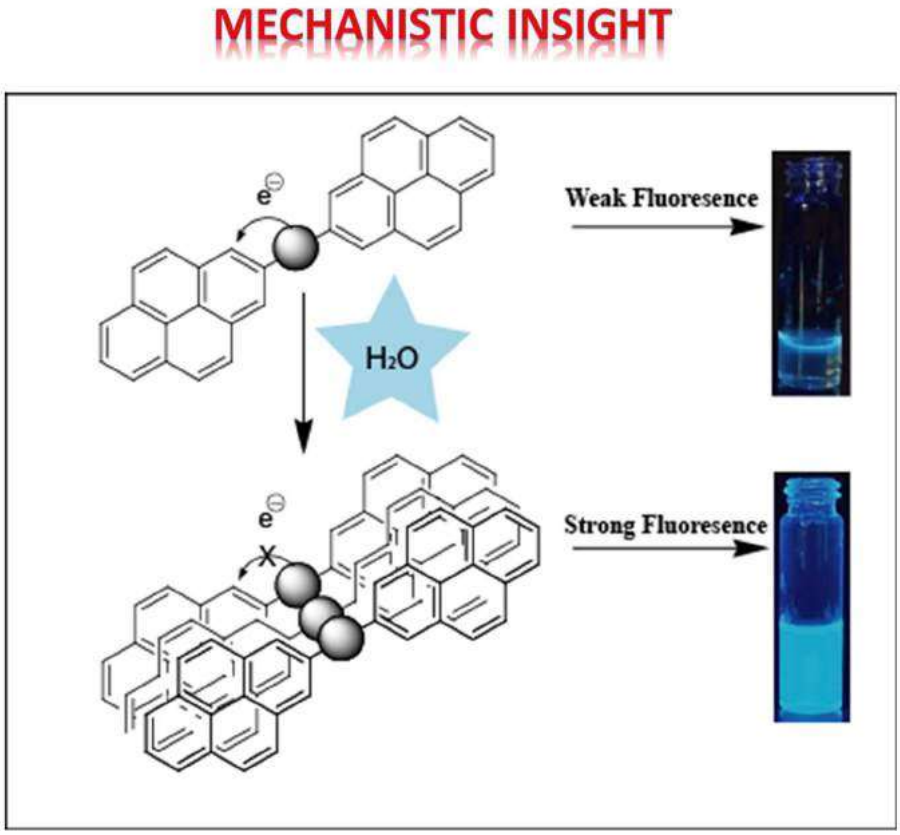

Figure 6.18 Plausible Mechanism of formation of aggregate among PRT with water